JACS Au
AN OPEN ACCESS JOURNAL OF THE AMERICAN CHEMICAL SOCIETY

pubs.acs.org/jacsau

Article

# Investigation of the Biosynthetic Mechanism of Bipentaromycin Featuring an Unprecedented Cyclic Head-to-Tail Dimeric Scaffold

Chunshuai Huang, Haiyang Cui, Hengqian Ren, and Huimin Zhao*

Cite This: *JACS Au* 2023, 3, 195−203

Read Online

ACCESS | Metrics & More | Article Recommendations | Supporting Information

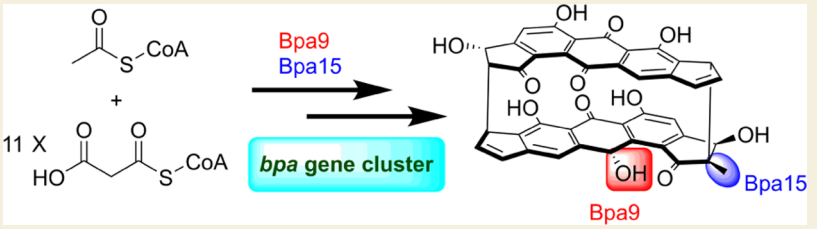


**ABSTRACT:** Bipentaromycins are heterodimeric aromatic polyketides featuring two distinctive 5/6/6/6/5 pentacyclic ring systems and exhibit antibacterial activities. However, their overall biosynthetic mechanism, particularly the mechanism for early-stage modifications, such as hydrogenation and methylation, and late-stage dimerization, remains unknown. Herein, by integrating heterologous expression, isotope labeling, gene knockout and complementation, and computational modeling, we determined the biosynthetic origin of the skeleton, identified the enzymes involved in stereo-/regioselective hydrogenation and methylation, and provided new mechanistic insights into the dimerization. This work not only deciphers the biosynthetic mechanism of bipentaromycins but also provides new strategies for creating biologically active dimeric pharmacophores for drug discovery and development.

**KEYWORDS:** *bipentaromycin, dimer, biosynthetic origin, stereospecific modification, computational modeling*

## INTRODUCTION

Natural products originated from microorganisms have a wide range of pharmacological properties and are a rich source of small-molecule drugs.[1] Various homo-/heterodimeric natural products with high scaffold diversity, structural complexity, and diverse bioactivities have been discovered from bacteria and fungi,[2] such as rugulin,[3] forrestiacids,[4] dinapinones,[5] secalonic acids,[6] actinorhodins,[7] lomaiviticins,[8] nenestatins B and D,[9] and difluostatins[10−12] (Figure 1). Notably, these dimeric molecules often exhibit more potent biological activities than their respective monomers and have greater potential to be therapeutic agents.[10,13,14] For example, the $C_2$-symmetric lomaiviticin A exhibited a 100-fold higher cytotoxicity than the monomeric kinamycin C against a variety of human cancer cell lines.[15,16] However, the biosynthetic mechanisms of most dimeric natural products remain unknown.[2]

Recently, we discovered several unprecedented dimeric aromatic polyketides named bipentaromycins in *Streptomyces* sp. NRRL F-6131, and four of them (bipentaromycins C−F) exhibited varying degrees of antibacterial activity against both Gram-positive and Gram-negative bacteria.[17] Notably, the structural complexity of bipentaromycins is mainly attributed to the anthraquinone core fused with two uncommon five-membered rings on both sides, the unexpected cyclic head-to-tail (C-2−C-8′ and C-8−C-2′) dimerization of two anthraquinone-based monomers, and the diverse modifications (e.g., selective hydrogenation, methylation, and acylation).

In this work, we investigated the biosynthetic mechanism of bipentaromycins. Specifically, using heterologous expression, isotope feeding, and genetic knockout and complementation, we not only discovered and characterized a total of 17 bipentaromycins and dodecaketide derivatives, but also determined the biosynthetic origin of bipentaromycin skeleton. Moreover, we gained a better understanding of selective catalytic hydrogenation and methylation and their corresponding biosynthetic enzymes as well as the dimerization mechanism by combining genetic experiments and computational modeling. This work provides new insights into constructing biologically active dimeric pharmacophores for drug discovery and development.

Received: October 30, 2022
Revised: December 17, 2022
Accepted: December 19, 2022
Published: December 30, 2022





https://doi.org/10.1021/jacsau.2c00594
*JACS Au* 2023, 3, 195−203

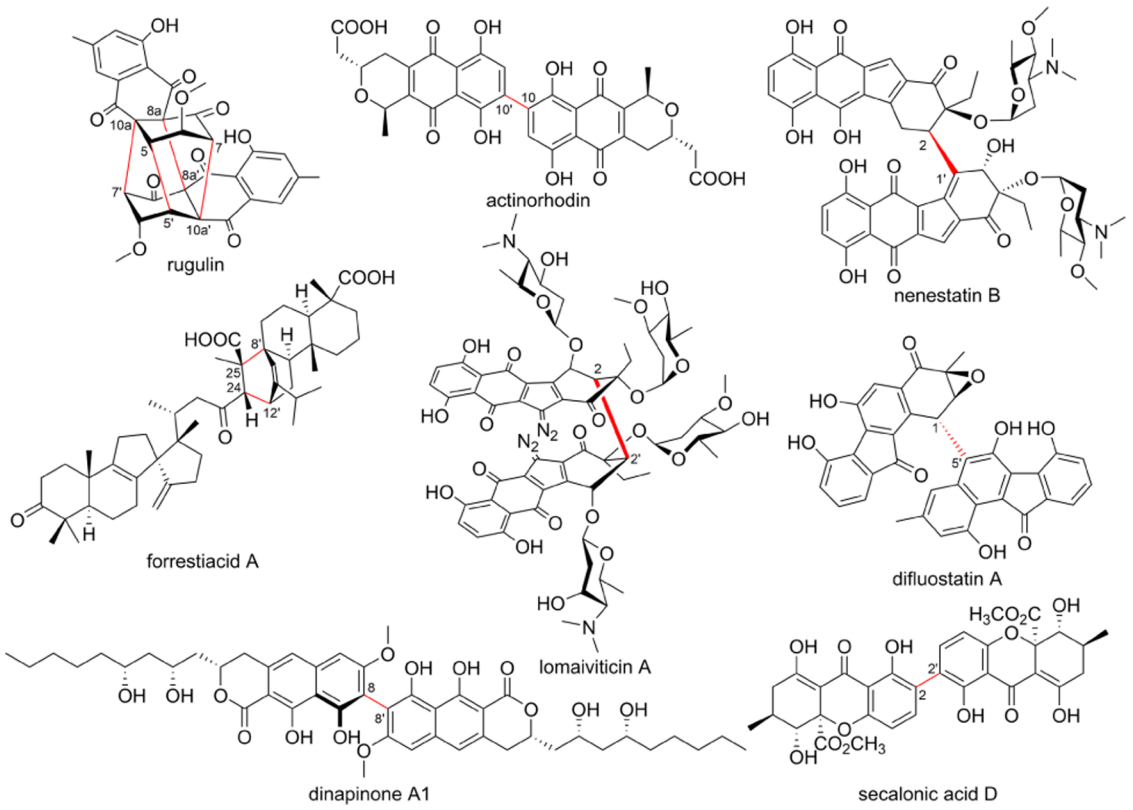


**Figure 1.** Representative dimeric molecules. The connections of dimeric scaffolds are labeled using red bonds.

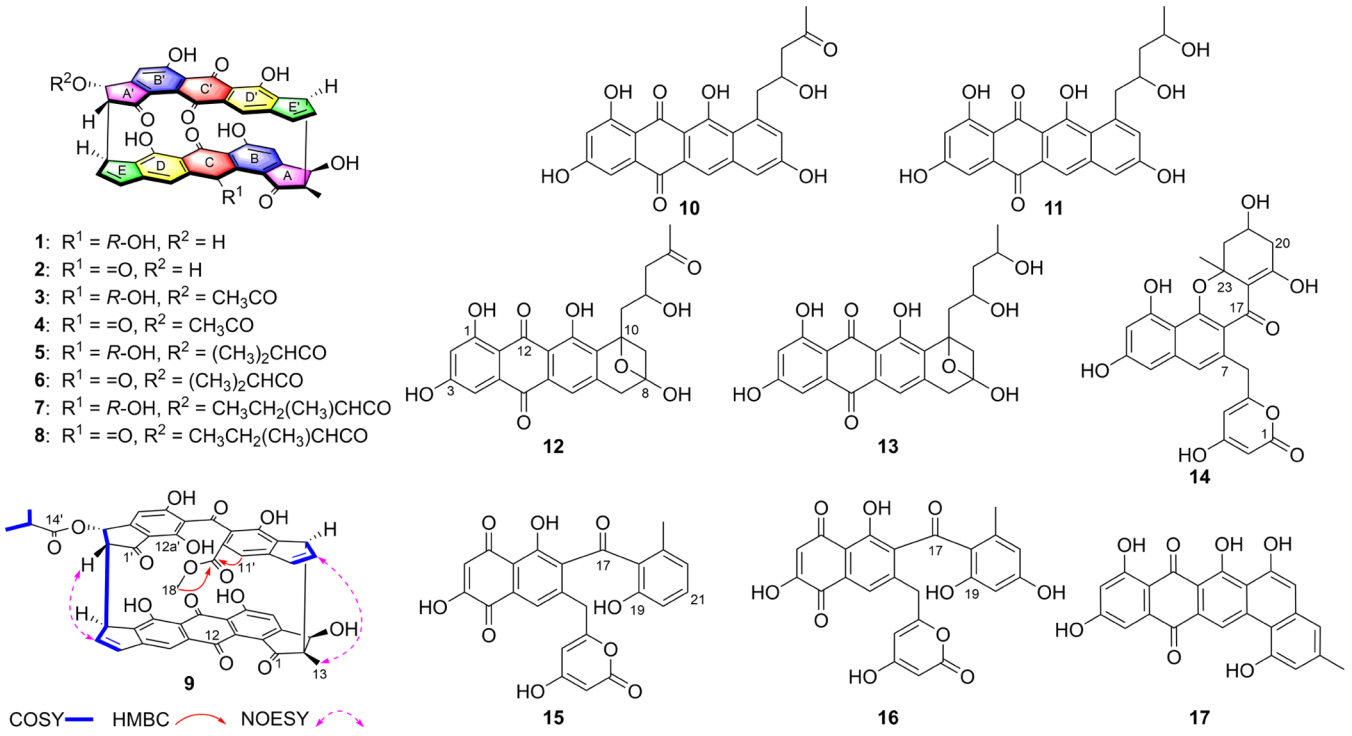


**Figure 2.** Secondary metabolites from *S. avermitilis* SUKA17 harboring the *bpa* gene cluster. Chemical structures of compounds **1**−**17**, as well as selected key COSY, HMBC, and NOESY correlations of **9**.



https://doi.org/10.1021/jacsau.2c00594
*JACS Au* 2023, 3, 195−203

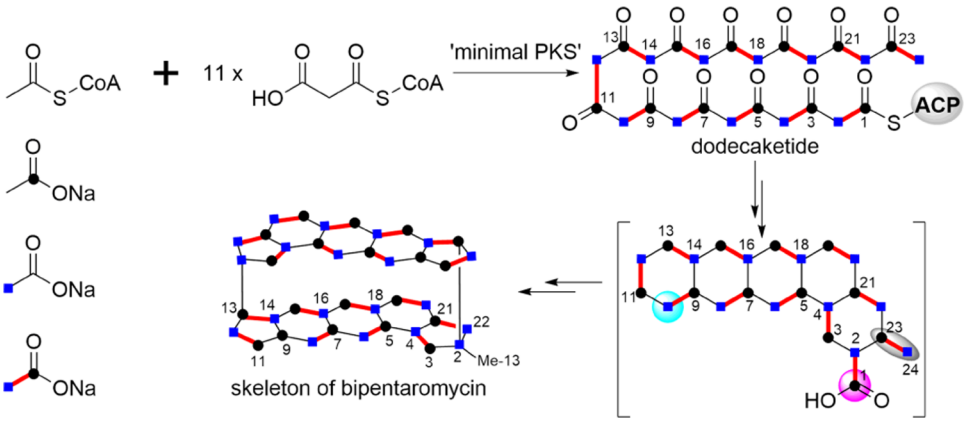


**Figure 3.** Labeling studies of bipentaromycins with [1-$^{13}$C]-, [2-$^{13}$C]- and [1,2-$^{13}C_2$]-sodium acetate, respectively. The missing carbons are highlighted with ellipsoids or spheres in brackets.

## RESULTS AND DISCUSSION

### Discovery and Structure Identification of Novel Bipentaromycins and Related Derivatives

Heterologous expression of the bipentaromycin biosynthetic gene cluster (BGC) (designated as *bpa*, Tables S1 and S2) in the model host *Streptomyces avermitilis* SUKA17 led to the production of 17 compounds (Figures 2 and S1), which were isolated and identified by high-performance liquid chromatography (HPLC), high-resolution electrospray ionization mass spectroscopy (HRESIMS), and nuclear magnetic resonance (NMR). These compounds include eight cyclic head-to-tail heterodimers bipentaromycins A−H (**1**−**8**), a derivative of bipentaromycin F (named as bipentaromycin I, **9**), and eight dodecaketide derivatives **10**−**17**.

Among the eight bipentaromycins, the six identified bipentaromycins A−F (**1**−**6**) agreed well with our previous study,[17] and two bipentaromycin congeners (**7** and **8**) bearing similar ultraviolet−visible (UV−vis) absorption (Figure S1) were additionally observed. After purification and structural characterization, compounds **7** and **8** were designated as bipentaromycins G and H, respectively (Table S3 and Figures S2 and S3). The molecular formula of bipentaromycin G (**7**) was determined as $C_{46}H_{32}O_{13}$ by the negative HRESIMS (*m*/*z*: found 791.1786 $[M-H]^-$, calcd 791.1770, Figure S2). Analyses of $^1$H and $^{13}$C NMR spectroscopic data (Table S3 and Figure S2) revealed that the structures of **7** and bipentaromycin E (**5**) were highly similar, yet the isobutyryl group in **5** was changed to a 2-methylbutyryl group in **7**. The latter was supported by COSY correlations of $H_3$-17′/$H_2$-16′/H-15′/$H_3$-18′ and HMBC correlations from $H_3$-18′ to C-14′/C-15′/C-16′ and $H_3$-17′ to C-15′/C-16 (Figure S2). Compared with **7**, a carbonyl group instead of the hydroxyl group was found to be located at C-12 in bipentaromycin H (**8**).

Interestingly, an unexpected trace component **9**, assigned as bipentaromycin I (**9**, Figures 2 and S1), was isolated and characterized as a derivative of bipentaromycin F (**6**). Bipentaromycin I (**9**) reveals high structural similarity to bipentaromycin F (**6**), except for an opened C′-ring suggested by NMR spectra (Table S3 and Figure S4). The HMBC correlations from H-11′ and $H_3$-18′ to C-12′ indicated that **9** was a C′-ring opening between C-12′ and C-12a′ and methyl esterification of bipentaromycin F (**6**) (Figure 2). In terms of eight dodecaketide derivatives **10**−**17** (Tables S4−S6 and Figures S5−S12), compounds **12**−**15** were characterized as novel aromatic polyketides, together with four known compounds A35566-A (**10**),[18] A35566-B (**11**),[18] TW95b (**16**),[19] and JX111b (**17**).[20]

### Deciphering the Biosynthetic Origin of Bipentaromycin Skeleton

To decipher and understand the biosynthetic origin of bipentaromycin skeleton, $^{13}$C-labeled precursors of [1-$^{13}$C]-, [2-$^{13}$C]-, and [1,2-$^{13}C_2$]-sodium acetates were fed to the fermentation culture of *S. avermitilis* SUKA17 harboring the *bpa* gene cluster in M-AM3-D medium,[21] respectively (Figure 3). In the [1-$^{13}$C]-sodium acetate feeding experiment, $^{13}$C NMR spectrum analysis of bipentaromycin C (**3**) revealed that 20 carbon signals (i.e., C3, C5, C7, C9, C11, C13, C15, C17, C19, C21, C3′, C5′, C7′, C9′, C11′, C13′, C15′, C17′, C19′, and C21′) were found to be significantly enriched compared with the unlabeled **3** (Figure S13). Besides, enriched carbon signals for bipentaromycin E (**5**) were observed at 20 different carbons in [2-$^{13}$C]-sodium acetate feeding experiment, including C2, C4, C6, C8, C12, C14, C16, C18, C20, C22, C2′, C4′, C6′, C8′, C12′, C14′, C16′, C18′, C20′, and C22′ (Figure S13). Further analysis of the $^{13}$C NMR spectrum of [1,2-$^{13}C_2$]-sodium acetate labeled **3** showed that all carbon resonances except Me-13 were enriched (Figure S13). All except C2, C9, C2′, and C9′ were coupled to one other carbon, in which carbons derived from the same sodium acetate unit shared the same $J_{CC}$ values (Table S7). Additionally, the single and enriched signals of C2, C9, C2′, and C9′ meant that they were nonpaired carbons, and their counterparts (C1, C10, C1′, and C10′) of the same acetate unit were lost. Surprisingly, the lack of enrichment of Me-13 by [2-$^{13}$C]-labeled sodium acetate in **5** implied that the only methyl group on the skeleton was post-loaded, and the initial starting unit acetyl-CoA was removed from the nascent dodecaketide chain during the biosynthesis of bipentaromycins (Figure 3). Collectively, feeding experiments with $^{13}$C-labeled sodium acetates unveil that the bipentaromycins appear to arise from the contraction and dimerization of a 6/6/6/6/6 pentacyclic ring precursor.

### Stereospecific Hydrogenation Catalyzed by Bpa8/Bpa9

The occurrence of structural complexity and diversity of natural products are largely attributed to enzymatic or nonenzymatic modifications, including cyclization, oxidoreduction, alkylation, acylation, glycosylation, dimerization, and rearrangement reactions.[22] Moreover, these distinctive and elaborate structural decorations, especially those with high regio-/stereoselectivity,


https://doi.org/10.1021/jacsau.2c00594
JACS Au 2023, 3, 195−203

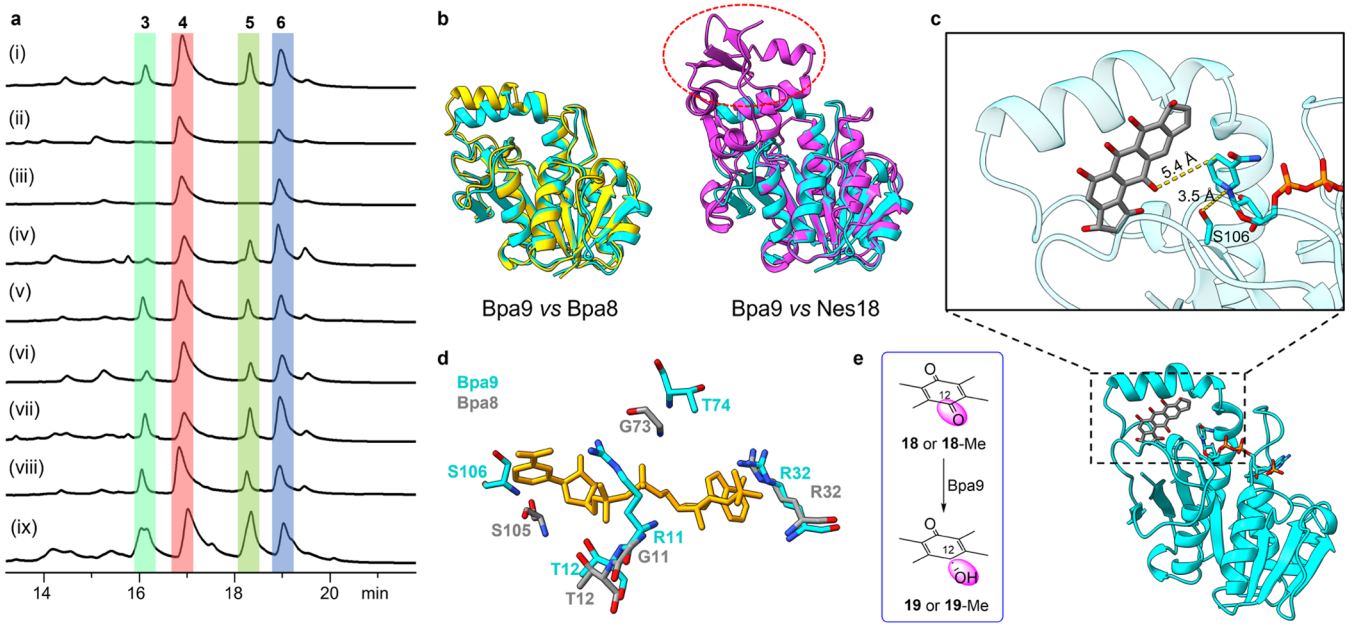


**Figure 4.** Investigation of the hydrogenation reaction in bipentaromycins. (a) HPLC profiles of deletion mutants and the mutants complementing Δ*bpa*9 and Δ*bpa*(8 + 9) with corresponding genes, respectively. (i) Δ*bpa*8; (ii) Δ*bpa*9; (iii) Δ*bpa*(8 + 9); (iv) Δ*bpa*9::*bpa*8; (v) Δ*bpa*9::*bpa*9; (vi) Δ*bpa*(8 + 9)::*bpa*8; (vii) Δ*bpa*(8 + 9)::*bpa*9; (viii) Δ*bpa*(8 + 9)::*bpa*(8 + 9); and (ix) F-6131 BGC *bpa* control. (b) Structure superimposition of Bpa9, Bpa8, and Nes18. Bpa9, Bpa8, and Nes18 are shown as cartoons with the color cyan, yellow, and pink, respectively. The red dotted circle highlights the distinguished difference between Bpa9 and Nes18. (c) A close-up view from the docking pose of substrate **18** in the substrate binding site of Bpa9 from the molecular docking study in catalytically competent orientation. The Bpa9 is shown in cyan with 90% transparency. Substrate **18** is shown in ball and stick representation, with carbon in dark gray, nitrogen in blue, and oxygen in red. The $NADP^+$ is represented as sticks. The nitrogen atoms are in blue, oxygen in red, and sulfur in orange. (d) Stick representation of the active site in Bpa9 overlaid with Bpa8. The residues in Bpa9 are labeled in cyan fonts, and the corresponding ones in Bpa8 are labeled in dark gray. (e) Bpa9-catalyzed hydrogenation reaction.

are also often associated with biological activity. Therefore, we sought to investigate the enzymology for the complex modifications involved in the monomeric building block of bipentaromycins.

Some redox enzymes have often been proposed to catalyze intra-/intermolecular C−C bond-forming reactions, such as the putative oxidoreductase HrbY-mediated dimerization.[23] To identify which enzyme is likely involved in the dimerization of bipentaromycins, we removed each of the seven redox enzyme-encoding genes (*bpa*11, *bpa*18, *bpa*19, *bpa*28, *bpa*30, *bpa*33, and *bpa*38) in the *bpa* BGC (Tables S1 and S8 and Figure S14) and then performed a comparative analysis of metabolite profiling chromatograms by HPLC (Figure S15). All of these mutants abrogated the production of bipentaromycins, except for the Δ*bpa*30 mutant, in which bipentaromycins were produced at a reduced level. Unexpectedly, though, only five off-pathway products (**10**−**14**) accumulated in mutants Δ*bpa*11, Δ*bpa*19, and Δ*bpa*33, and compound **17** was accumulated in mutant Δ*bpa*38 (Figure S15). Despite trying very hard, we did not get any monomeric structure of bipentaromycins, probably due to the highly unstable and reactive intermediates.

The NmrA family regulatory proteins ActVA-ORF4, Lom19, and Nes18 have been implicated as dimerization enzymes in the biosynthesis of actinorhodins, lomaiviticins, and nenestatins B and D, respectively. In our case, genes *bpa*8 and *bpa*9 found in the *bpa* BGC were also predicted to encode the NmrA family proteins, showing approximately 40% amino acid sequence similarities with ActVA-ORF4/Lom19/Nes18 (Table S9). Surprisingly, *bpa*9 and *bpa*(8 + 9) gene deletions abolished the production of bipentaromycins with a hydroxy group at C-12 (e.g., **3** and **5**, Figure 4a) rather than the effect on the production of all dimeric bipentaromycins. As expected, bipentaromycin production was completely restored by the complementation of *bpa*9 in the Δ*bpa*9 mutant. Interestingly, the *bpa*8 gene only partially complemented the Δ*bpa*9 mutant to produce bipentaromycins (Figure 4a). Subsequent complementation experiments of Δ*bpa*(8 + 9) mutant with *bpa*9 and *bpa*(8 + 9), respectively, also recovered the production of bipentaromycins (Figure 4a). In contrast, the complementation of Δ*bpa*(8 + 9) mutant with *bpa*8 showed almost the same production profile as that in Δ*bpa*9 mutant complemented with *bpa*8 (Figure 4a). The latter suggests that *bpa*8 could partially complement the function of *bpa*9, but it is not essential for the production of bipentaromycins. Thus, *bpa*8 and *bpa*9 were deduced to be associated with the stereospecific hydrogenation of the carbonyl group at C-12 in bipentaromycins.

To better understand the functions of Bpa8 and Bpa9, we performed computational modeling studies. The three-dimensional (3D) structures of Bpa8, Bpa9, ActVA-ORF4, Lom19, and Nes18 were predicted by AlphaFold[24] with high confidence (Figures 4b and S16). As shown in Figures 4b and S17, both 3D structures of Bpa8 and Bpa9 lacked a common C-terminal domain that appeared within ActVA-ORF4/Lom19/Nes18. Interestingly, when overlaying the Bpa9 (or Bpa8) with the homologous Biliverdin IX$\beta$ Reductase B,[25] the most noticeable difference is the extended $\alpha$-helix (residue 115−126 in Bpa9 and residue 116−128 in Bpa8, Figure S18). The docking study demonstrated that the extended $\alpha$-helix might have an important role in enabling the putative monomer **18**, half of bipentaromycin, to bind to the active site (Figure 4c). The catalytic residues in the active site within NAD(P)H-dependent reductases Bpa9 and Bpa8 were determined by combining evolutionary conservation analysis and structure alignment (Figures S18 and S19). Stabilization of the 2′-phosphate group


https://doi.org/10.1021/jacsau.2c00594
JACS Au 2023, 3, 195−203

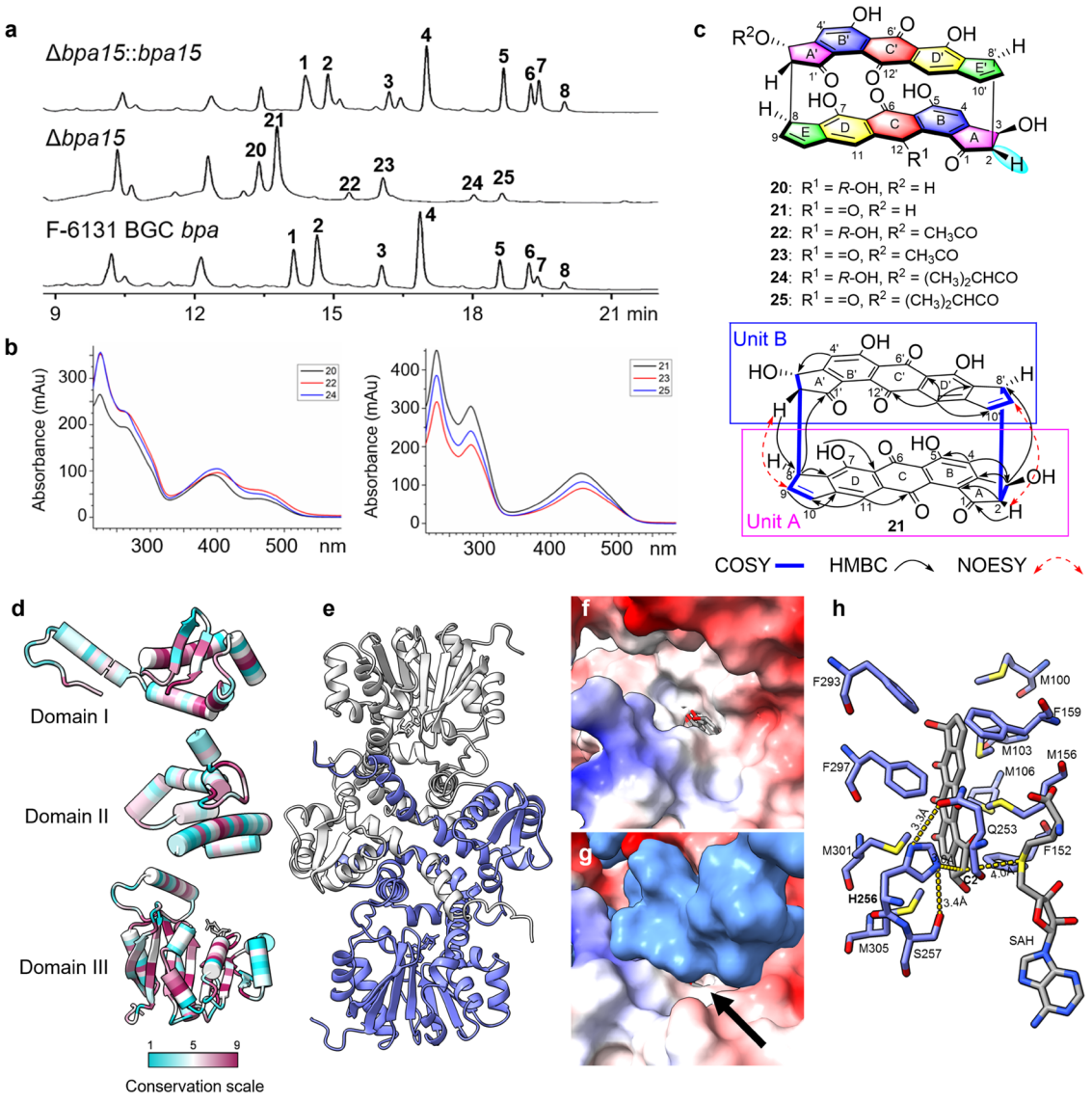


**Figure 5.** HPLC profiles, product characterization, and computational modeling study. (a) HPLC profiles of mutant Δ*bpa*15 and the mutant complementing the Δ*bpa*15 mutant with *bpa*15. (b) UV−vis absorption of 2-demethylbipentaromycins A−F (**20**−**25**). (c) Chemical structures of isolated compounds from mutant Δ*bpa*15. (d) Structure of the Bpa15 monomer. Secondary structure diagram of the Bpa15 monomer separated by domain and colored with evolutionary conservation scores. Amino acid conservation scores are shown using the color-coding bar in which highly variable and conserved residues are shown in cyan and red, respectively. Evolutionary conservation analysis of Bpa15 was performed using the ConSurf online server. (e) Bpa15 dimer, with one subunit colored purple and the other colored gray. (f, g) Substrate binding pocket of Bpa15 with **18** fitted into the structure by autodocking. Surface representations of Bpa15 viewed from the protein−solvent interface toward the substrate binding site (f) with and (g) without the second monomer of the dimer, respectively. The black arrow indicates the proposed narrow substrate entry tunnel. The surface presentation is colored by electrostatic potential. The positive charge is shown in blue, and the negative charge is shown in red. The surface is colored purple for the second monomer for clarity. (h) Local environment at the substrate binding site. The carbon atoms are colored purple for the amino acid residues and gray for SAH and **18**. SAH, **18**, and the amino acid residues within 3.5 Å of **18** are represented by sticks.

of $NADP^+$ is achieved by a hydrogen bond to the side chains of Arg32 and Thr74 within Bpa9. However, such a hydrogen bond cannot be found in Bpa8 because the amino acid Thr74 in Bpa9 was replaced with Gly73 in Bpa8 (Figure 4d). Taken together, Bpa8 and Bpa9 are responsible for the stereospecific hydrogenation of the carbonyl group at C-12 to yield the corresponding alcohols (**19** and **19**-Me) in the early-stage modification of bipentaromycins (Figure 4e).

## Bpa15 Functions as a *C*-Methyltransferase

As mentioned above, $^{13}C$-labeling experiments indicated that the installation of the methyl group was a post-modification process, so a putative *C*-methyltransferase was hypothesized to be involved in the formation of bipentaromycins. However, bioinformatics analysis showed that no *C*-methyltransferase-encoding gene was found in the *bpa* BGC. Alternatively, a putative *S*-adenosine methionine (SAM) dependent *O*-methyltransferase-encoding gene *bpa*15 was proposed to be responsible for the methylation step in the bipentaromycin biosynthesis. By deleting the *bpa*15 (Table S8 and Figure S14), we did not observe any production of bipentaromycins A−H (**1**−**8**). Instead, six distinct peaks were significantly accumulated in the Δ*bpa*15 mutant (Figure 5). Analysis of the metabolite profiles using high-performance liquid chromatography-diode array detection (HPLC−DAD) suggested that they had a close


https://doi.org/10.1021/jacsau.2c00594
JACS Au 2023, 3, 195−203

**Scheme 1. Proposed Biosynthetic Mechanism for the Dimerization of Bipentaromycins**

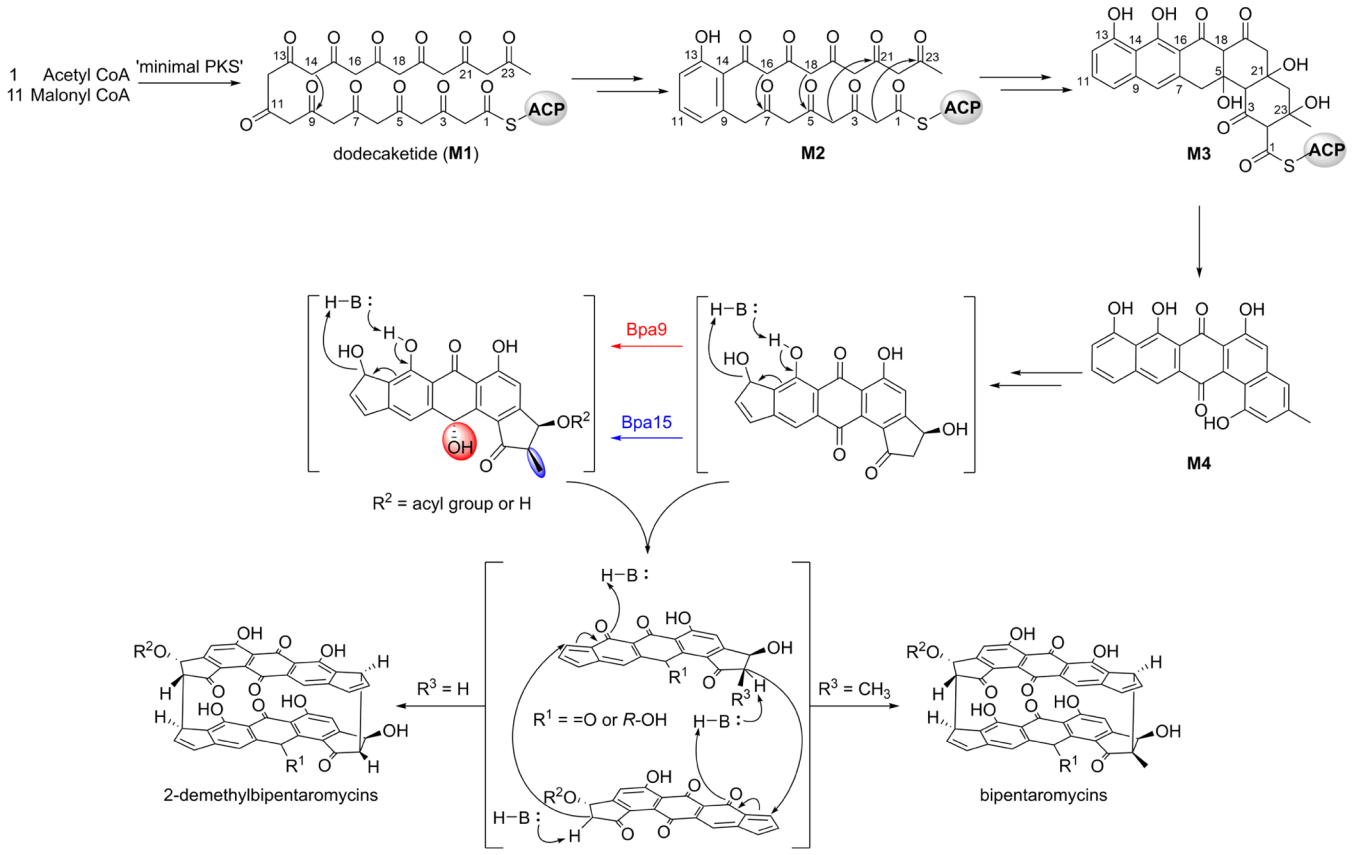


structural relationship with bipentaromycins (Figures 2 and 5). Upon UV−vis-guided purification by reversed-phase semi-preparative HPLC, a total of six analogues were isolated from a 3.0 L culture of Δ*bpa*15 mutant. HRESIMS coupled with NMR data (Tables S11 and S12 and Figures S20−S25) allowed us to identify them as 2-demethylbipentaromycins A−F (**20**−**25**). One of these 2-demethylbipentaromycins was characterized as a symmetric dimer and named as 2-demethylbipentaromycin B (**21**). It was obtained as a red amorphous powder with a molecular formula $C_{40}H_{20}O_{12}$ established by HRESIMS (*m*/*z* 691.0898 $[M - H]^-$, calcd 691.0882, Figure S21), corresponding to 31 degrees of unsaturation. The $^1H$ and $^{13}C$ NMR data (Table S11 and Figure S20) of **21** were highly similar to those of **2**,[17] indicating that **21** was an analogue of **2** containing the rare cyclic head-to-tail 5/6/6/6/5 pentacyclic carbon skeleton. The major differences were that the singlet methyl group ($\delta_H$ 1.57/$\delta_C$ 22.1) and the aliphatic quaternary carbon ($\delta_C$ 62.2) in **2** were not observed in **21**. Simultaneously, an additional methine signal ($\delta_H$ 3.52/$\delta_C$ 58.1) appeared in **21**. These assignments were strongly supported by the $^1H-^1H$ COSY correlations of H-3/H-2/H-8′ and the HMBC correlations from H-2 to C-1/C-3/C-3a/C-12b/C-7a′/C-8′/C-9′ (Figure 5). The NOESY correlation of H-2 with H-9′ indicated that they were in the same orientation. Similarly, H-9 and H-2′ were also in the same orientation. Finally, biogenetically, the absolute configuration of **21** was assigned as 2*R*, 3*S*, 8*S*, 2′*R*, 3′*S*, 8′*S*.

To further decipher the methylation mechanism of the identified *C*-methyltransferase Bpa15, we performed computational modeling studies as we did with Bpa8 and Bpa9. The Bpa15 monomer structure predicted by AlphaFold with high confidence indicates that Bpa15 indeed has the methyltransferase fold (Figure S26) and folds into three domains, as shown in Figure 5d: domain I (the N-terminal domain, residues 1−86) contains one small $\beta$-sheet of two 4-residue strands and five helices; domain II is all helical (residues 87−164); domain III (C-terminal domain, residues 165−349) has a Rossmann-like fold consisting of a $\beta$-sheet with seven strands and is predominately involved in cofactor SAM/substrate binding. Bpa15 possesses the highly conserved DXGXGXG motif (residues 182−188) that defines the SAM binding site of methyltransferase enzymes (Figures 5d and S27). The typical N-terminal domain suggests Bpa15, unlike the majority of structurally characterized small-molecule methyltransferases (Figure S28), is most likely a dimer, which is further confirmed by the AlphaFold-Multimer prediction tool and molecular weight analysis (Figures 5e and S26). Therefore, the N-terminal dimerization domain forms an extensive intertwined interface as well as contributes elements of the substrate binding site of the opposite subunit (Figure 5f,g). Based on HHpred homologue analysis and structural alignments, it was found that phenazine methyltransferase (LaPhzM; r.m.s.d. 1.91 Å[26]), carminomycin methyltransferase (DnrK; r.m.s.d. 3.57 Å[27]), and orsellinic acid methyltransferase (CalO1; r.m.s.d. 5.83 Å[28]) are structurally similar to Bpa15. Based on these similarities and docking results shown in Figure 5h, we postulated that His256 is the catalytic residue in Bpa15, with Gln253 and Ser257 mediating the proper orientation of His256 for deprotonation of the substrate C-2 position. More details are described in the Supporting Information Text. Taken together, Bpa15 is responsible for the regioselective installation of a methyl group to C-2, and it is a *C*-methyltransferase rather than an *O*-methyltransferase.


https://doi.org/10.1021/jacsau.2c00594
JACS Au 2023, 3, 195−203

### Investigating the Dimerization Mechanism of Bipentaromycins

Aromatic polyketides are a structurally diverse group of natural products which are usually biosynthesized by type II polyketide synthases (PKSs). The iterative type II PKS consists of the $\beta$-ketoacyl synthase subunits $KS_\alpha$ and $KS_\beta$, as well as an acyl carrier protein (ACP), namely, "minimal PKS".[22,29] It catalyzes one unit of acetyl-CoA and 11 units of malonyl-CoA to undergo iteratively decarboxylative Claisen condensation to generate the linear poly-$\beta$-ketone chain dodecaketide (**M1**), which is subsequently converted into **M2** sharing a characteristic C11 lacking the hydroxyl group and C9/C14 first-ring cyclization by keto reductase and aromatase/cyclase (Scheme 1). **M2** is proposed to be catalyzed by cyclases and oxygenases to generate **M4** via an intermediate **M3** with C9/C14, C7/C16, C5/C18, C4/C21, and C2/C23 cyclizations. We postulate that **M4** is an essential putative precursor for the formation of 2-demethylbipentaromycins and bipentaromycins through multistep reactions involving complex ring contraction, redox reaction, and dimerization. As shown above, Bpa9-catalyzed ketoreduction process and Bpa15-catalyzed methylation could give corresponding highly selective hydrogenation and methylation products, respectively. Notably, the formation of the *ortho*-quinone methide catalyzed by enzyme or non-enzyme initiated the 1,4-Michael addition step, which might be employed for the dimerization of bipentaromycins. This process is highly similar to the formation of difluostatins and nenestatins B and D.[9,11] However, probably due to the unexpected instability and reactivity of the true precursor, we failed to detect any accumulation of bipentaromycin monomers.

Alternatively, the unreduced nascent polyketide chain **M1** could be converted to C9/C14 cyclized aromatic intermediate **M5** with the hydroxyl group at C11 by downstream aromatase/cyclase (Scheme S1). Enzyme-catalyzed or spontaneous cyclization via aldol condensation[30,31] results in the conversion of **M5** to **M6** with C9/C14, C7/C16, C5/C18, and C2/C19 cyclizations. Then, **M6** is branched into different products **10**/**11** and **12**/**13**. Compounds **10** and **11** are presumed to be derived from the aromatization of the fourth ring of **M6**. Instead, it is speculated that **M6** could undergo a nucleophilic addition at C3 to afford two hemiketal products **12** and **13**. In addition, the single aromatic ring intermediate **M5** can be catalyzed by a cyclase to form **M7** containing the second aromatic ring,[32,33] which is then cyclized at C1-OH/C5 and C18/C23 to produce **15** and **16**. **M7** is hypothesized to generate the rare xanthone-containing compound **14** via C1-OH/C5, C18/C23, and C15-OH/C23 cyclizations. Moreover, the intermediate **M5** could be folded and cyclized, similar to that of **M4** biosynthesis to yield JX111b (**17**).

## CONCLUSIONS

In this study, a structurally fascinating heterodimer bipentaromycin I (**9**) and two new bipentaromycin congeners bipentaromycins G (**7**) and H (**8**), as well as eight dodecaketide derivatives **10**−**17** have been isolated and identified from the heterologous expression of the *bpa* gene cluster in *S. avermitilis* SUKA17. Bipentaromycin I (**9**) represents an unusual framework with a cleaved C′-ring. It is speculated that the C′-ring-cleaved product is produced by Baeyer−Villiger oxidation-mediated ring excision reaction.[34] The accumulation of **10**−**17** might be due to the spontaneous and aberrant cyclization of the highly reactive poly-$\beta$-ketone chain and the instability of intermediates.[35] Notably, compound **14** possesses a rare xanthone scaffold, a family of natural products known for their pronounced biological activity.[36] Additionally, the labeled sodium acetate feeding studies allow us to understand the potential biosynthetic logic for bipentaromycins. Structural alignments with known methyltransferases show that Bpa15 is most similar to the bacterial *O*-methyltransferases that are characterized by an unusual intertwined dimer interface. However, based on a comparative computational modeling study, labeled-precursor feeding experiments, and *in vivo* genetic experiments, Bpa15 was determined to be a *C*-methyltransferase responsible for the regioselective installation of the methyl group of bipentaromycins.

Some NmrA family of regulatory proteins, such as ActVA-ORF4,[7] Lom19,[8] and Nes18,[9] have been previously proposed to be responsible for the dimerization of actinorhodins, lomaiviticins, and nenestatins B and D, respectively, via hydroquinone, cyclohexanone, and quinone methide-like intermediate. However, *in vivo* gene knockout and complementation of NmrA family regulatory protein-encoding genes *bpa*8 and *bpa*9 demonstrate that both are involved in the selective hydrogenation of the carbonyl group at C-12 in bipentaromycins. Given that these NmrA family proteins have also been annotated as nicotinamide adenine dinucleotide (NAD) cofactor-binding regulatory proteins, and the formation of C−C/C−N coupled difluostatins was confirmed to be a nonenzymatic process and unrelated to the enzyme FlsQ1,[11] more solid experimental evidence is still needed to unambiguously clarify the specific dimerization function of the NmrA family proteins.

In summary, this study highlights the structural diversity of bipentaromycins, determines the biosynthetic origin of the skeleton, and provides new insights into the asymmetric hydrogenation and methylation of bipentaromycins as well as the dimerization mechanism. It has laid a solid foundation for further characterization and engineering of bipentaromycins for basic and applied biological research and medicine.

## METHODS

### General Experimental Procedures and Methodology

General materials and methods are summarized in Supporting Information Materials and Methods. Bacteria strains and plasmids used in this study are summarized in Table S2. Primers used in this study are listed in Table S8.

### Fermentation, Extraction, and Isolation

The fermentation of *S. avermitilis* SUKA17 harboring the *bpa* gene cluster was performed in MYM medium (malt extract 10 g $L^{-1}$, yeast extract 4 g $L^{-1}$, maltose 4 g $L^{-1}$, pH 7.2−7.4) at 28 °C for 3−5 days. Fermentation cultures (5.0 L) were harvested and separated into supernatants and mycelia by centrifugation. The supernatants were extracted with an equal volume of ethyl acetate. After the removal of the ethyl acetate by evaporation under vacuum, the crude extract was further separated and purified by semi-preparative HPLC to afford compounds **7** (4.7 mg), **8** (3.4 mg), **9** (1.8 mg), **10** (1.5 mg), **11** (1.7 mg), **12** (1.2 mg), **13** (2.0 mg), **14** (25.5 mg), **15** (2.2 mg), **16** (2.8 mg), and **17** (3.1 mg).

### Feeding Studies with $^{13}$C-Sodium Acetate

A total of 1 L culture was performed in a modified AM3-D medium (glucose 15 g $L^{-1}$, soybean flour 5 g $L^{-1}$, peptone 10 g $L^{-1}$, $CaCO_3$ 2 g $L^{-1}$) and was incubated on a rotary shaker (250 rpm) at 28 °C for 6 days. The $^{13}$C-labeled sodium acetate was added into the cultures at 24 and 48 h, respectively, at a final concentration of 2−3 mg $mL^{-1}$. The fermentation cultures were harvested and separated into supernatants and mycelia by centrifugation. The supernatant was extracted with an


https://doi.org/10.1021/jacsau.2c00594
JACS Au 2023, 3, 195−203

equal volume of ethyl acetate. The crude extract was further purified using semi-preparative HPLC.

### Gene Inactivation and Complementation

The *bpa*8, *bpa*9, *bpa*11, *bpa*15, *bpa*18, *bpa*19, *bpa*28, *bpa*30, *bpa*33, *bpa*38, and *bpa*(8 + 9) genes were individually inactivated (Figure S14). The positive plasmid was obtained and subsequently transformed into *Escherichia coli* WM6026, which was used as a donor strain to conjugate with the recipient *S. avermitilis* SUKA17. For gene complementation, the complement fragment was amplified by PCR using the pCHZ2021 as a template. The resulting fragment was assembled with the plasmid of pIJ10257 (digested with *Nde*I) utilizing Gibson assembly. Then, the assembly mixture was introduced into *E. coli* NEB10$\beta$ and screened with hygromycin resistance ($hyg^r$).

### Protein Structure Prediction and Molecular Docking

AlphaFold[24] was used to predict the three-dimensional structures of enzymes Bpa15, Bpa9, ActVA-ORF4, Lom19, and Nes18. Molecular docking studies were carried out to understand the catalytically competent docking poses of substrates. More details are described in the Supporting Information Methods.

### Overexpression, Purification, and Analysis of Bpa15

The *bpa*15 gene was PCR-amplified from the plasmid pCHZ2021 and cloned into the vector pET28a. After sequencing confirmation, the recombinant plasmid was introduced into *E. coli* BL21(DE3) to produce the *N*-$(His)_6$-tagged Bpa15 protein. Single colony was used to inoculate 5 mL LB medium containing 50 $\mu g\ mL^{-1}$ kanamycin and grown overnight at 37 °C at 250 rpm. Each 100 mL of fresh LB medium with the same antibiotic selection was inoculated with 1 mL of the overnight culture and incubated at 37 °C until the optical density at 600 nm ($OD_{600}$) reached 0.4−0.6. Protein expression was induced with 0.2 mM isopropyl-$\beta$-D-thiogalactopyranoside (IPTG), followed by further incubation for 18−24 h at 16 °C. *E. coli* cells were harvested by centrifugation at 8000 rpm at 4 °C for 10 min, washed with deionized water, and suspended in 20 mM Tris-Cl, 1 M NaCl, followed by sonication on ice. Lysed cells were centrifuged at 14,000 rpm for 50 min at 4 °C to remove cellular debris. The supernatant, as crude enzyme, was purified with the following gradient buffer system: buffer A (20 mM Tris-Cl, 1 M NaCl) and buffer B (20 mM Tris-Cl, 1 M NaCl, 500 mM imidazole) from 0% B to 100% B. The elute containing the purified enzyme was immediately desalted with buffer A. The molecular weight ($M_W$) of recombinant protein was analyzed by sodium dodecyl sulfate−polyacrylamide gel electrophoresis (SDS-PAGE) and gel filtration.

## ■ ASSOCIATED CONTENT

### Supporting Information

The Supporting Information is available free of charge at https://pubs.acs.org/doi/10.1021/jacsau.2c00594.

Detailed computational studies on enzyme mechanisms; materials and methods; strains, plasmids, and primers used in this study; MS and NMR spectroscopic data for compounds **7**−**17**, and **20**−**25**; predicted protein structures; protein structure modeling; and supporting references (PDF)

## ■ AUTHOR INFORMATION


### Corresponding Author

**Huimin Zhao** − *Carl R. Woese Institute for Genomic Biology, University of Illinois at Urbana-Champaign, Urbana, Illinois 61801, United States; Department of Chemical and Biomolecular Engineering, Department of Biochemistry, and Department of Chemistry, University of Illinois at Urbana-Champaign, Urbana, Illinois 61801, United States;* orcid.org/0000-0002-9069-6739; Phone: (217) 333-2631; Email: zhao5@illinois.edu; Fax: (217) 333-5052

### Authors

**Chunshuai Huang** − *Carl R. Woese Institute for Genomic Biology, University of Illinois at Urbana-Champaign, Urbana, Illinois 61801, United States;* orcid.org/0000-0002-3126-2340

**Haiyang Cui** − *Carl R. Woese Institute for Genomic Biology, University of Illinois at Urbana-Champaign, Urbana, Illinois 61801, United States;* orcid.org/0000-0001-8360-0447

**Hengqian Ren** − *Department of Chemical and Biomolecular Engineering, University of Illinois at Urbana-Champaign, Urbana, Illinois 61801, United States*

Complete contact information is available at: https://pubs.acs.org/10.1021/jacsau.2c00594


### Author Contributions

C.H. performed compound isolation, structure determination, and labeling study. H.C. performed the protein structure prediction and computational modeling. C.H. and H.R. conducted the *in vivo* genetic studies. C.H. and H.C. analyzed the data and wrote the manuscript. H.Z. directed the research. All authors reviewed and gave approval to the final version of the manuscript.

### Notes

The authors declare no competing financial interest.

## ■ ACKNOWLEDGMENTS

The authors thank Xudong Guan and Leonardo Vazquez (Carl R. Woese Institute for Genomic Biology) for NMR measurement and Furong Sun (School of Chemical Sciences Mass Spectrometry Laboratory) for HRESIMS data analysis. The authors are grateful to Zengfei Pei for molecular weight analysis of Bpa15. Some of these data were collected in the Carl R. Woese Institute for Genomic Biology Core on a 600 MHz NMR funded by NIH grant number S10-RR028833. This work was supported by the grants GM077596 and AI144967 from the National Institutes of Health (H.Z.).

## ■ REFERENCES


(1) Hobson, C.; Chan, A. N.; Wright, G. D. The antibiotic resistome: A guide for the discovery of natural products as antimicrobial agents. *Chem. Rev.* **2021**, *121*, 3464−3494.

(2) Liu, J.; Liu, A.; Hu, Y. Enzymatic dimerization in the biosynthetic pathway of microbial natural products. *Nat. Prod. Rep.* **2021**, *38*, 1469−1505.

(3) Han, Y. B.; Bai, W.; Ding, C. X.; Liang, J.; Wu, S.-H.; Tan, R. X. Intertwined biosynthesis of skyrin and rugulosin A underlies the formation of cage-structured bisanthraquinones. *J. Am. Chem. Soc.* **2021**, *143*, 14218−14226.

(4) Xiong, J.; Zhou, P.; Jiang, H.; Huang, T.; He, Y.; Zhao, Z.; Zang, Y.; Choo, Y.; Wang, X.; Chittiboyina, A. G.; Pandey, P.; Hamann, M. T.; Li, J.; Hu, J. F. Forrestiacids A and B, pentaterpene inhibitors of ACL and lipogenesis: Extending the limits of computational NMR methods in the structure assignment of complex natural products. *Angew. Chem., Int. Ed.* **2021**, *60*, 22270−22275.

(5) Kawaguchi, M.; Ohshiro, T.; Toyoda, M.; Ohte, S.; Inokoshi, J.; Fujii, I.; Tomoda, H. Discovery of a fungal multicopper oxidase that catalyzes the regioselective coupling of a tricyclic naphthopyranone to produce atropisomers. *Angew. Chem.* **2018**, *130*, 5209−5213.

(6) Wei, X.; Chen, X.; Chen, L.; Yan, D.; Wang, W.-G.; Matsuda, Y. Heterologous biosynthesis of tetrahydroxanthone dimers: Determination of key factors for selective or divergent synthesis. *J. Nat. Prod.* **2021**, *84*, 1544−1549.

(7) Taguchi, T.; Ebihara, T.; Furukawa, A.; Hidaka, Y.; Ariga, R.; Okamoto, S.; Ichinose, K. Identification of the actinorhodin monomer

and its related compound from a deletion mutant of the *act*VA-ORF4 gene of *Streptomyces coelicolor* A3(2). *Bioorg. Med. Chem. Lett.* **2012**, *22*, 5041−5045.
(8) Janso, J. E.; Haltli, B. A.; Eustaquio, A. S.; Kulowski, K.; Waldman, A. J.; Zha, L.; Nakamura, H.; Bernan, V. S.; He, H.; Carter, G. T.; Koehn, F. E.; Balskus, E. P. Discovery of the lomaiviticin biosynthetic gene cluster in *Salinispora pacifica*. *Tetrahedron* **2014**, *70*, 4156−4164.
(9) Jiang, X.; Fang, Z.; Zhang, Q.; Liu, W.; Zhang, L.; Zhang, W.; Yang, C.; Zhang, H. B.; Zhu, Y.; Zhang, C. Discovery of a new asymmetric dimer nenestatin B and implications of dimerizing enzyme in a deep sea actinomycete. *Org. Biomol. Chem.* **2021**, *19*, 4243−4247.
(10) Yang, C.; Huang, C.; Zhang, W.; Zhu, Y.; Zhang, C. Heterologous expression of fluostatin gene cluster leads to a bioactive heterodimer. *Org. Lett.* **2015**, *17*, 5324−5327.
(11) Huang, C.; Yang, C.; Zhang, W.; Zhang, L.; De, B. C.; Zhu, Y.; Jiang, X.; Fang, C.; Zhang, Q.; Yuan, C.-S.; Liu, H.-w.; Zhang, C. Molecular basis of dimer formation during the biosynthesis of benzofluorene-containing atypical angucyclines. *Nat. Commun.* **2018**, *9*, No. 2088.
(12) Huang, C.; Yang, C.; Zhang, W.; Zhang, L.; Zhu, Y.; Zhang, C. Discovery of an unexpected 1,4-oxazepine-linked *seco*-fluostatin heterodimer by inactivation of the oxidoreductase-encoding gene *flsP*. *J. Nat. Prod.* **2021**, *84*, 2336−2344.
(13) Fernandes, R. A.; Patil, P. H.; Chaudhari, D. A. Dimeric pyranonaphthoquinones: Isolation, bioactivity, and synthetic approaches. *Eur. J. Org. Chem.* **2016**, *2016*, 5778−5798.
(14) Jung, M.; Lee, S.; Ham, J.; Lee, K.; Kim, H.; Kim, S. K. Antitumor activity of novel deoxoartemisinin monomers, dimers, and trimer. *J. Med. Chem.* **2003**, *46*, 987−994.
(15) Herzon, S. B. The mechanism of action of (−)-lomaiviticin A. *Acc. Chem. Res.* **2017**, *50*, 2577−2588.
(16) Colis, L. C.; Woo, C. M.; Hegan, D. C.; Li, Z.; Glazer, P. M.; Herzon, S. B. The cytotoxicity of (−)-lomaiviticin A arises from induction of double-strand breaks in DNA. *Nat. Chem.* **2014**, *6*, 504−510.
(17) Enghiad, B.; Huang, C.; Guo, F.; Jiang, G.; Wang, B.; Tabatabaei, S. K.; Martin, T. A.; Zhao, H. Cas12a-assisted precise targeted cloning using *in vivo* Cre-*lox* recombination. *Nat. Commun.* **2021**, *12*, No. 1171.
(18) Ogawa, J.; Kurakata, S.; Kaneko, I.; Tamaki, K.; Negishi, T.; Enokida, R.; Kinoshita, T.; Kuwano, H. JP07316091A, 1995-12-05, 1995.
(19) Yu, T.-W.; Shen, Y.; McDaniel, R.; Floss, H. G.; Khosla, C.; Hopwood, D. A.; Moore, B. S. Engineered biosynthesis of novel polyketides from *Streptomyces* spore pigment polyketide synthases. *J. Am. Chem. Soc.* **1998**, *120*, 7749−7759.
(20) Zhan, J.; Watanabe, K.; Tang, Y. Synergistic actions of a monooxygenase and cyclases in aromatic polyketide biosynthesis. *ChemBioChem* **2008**, *9*, 1710−1715.
(21) Zheng, L.; Jiang, X.; Zhang, Q.; Zhu, Y.; Zhang, H.; Zhang, W.; Saurav, K.; Liu, J.; Zhang, C. Discovery and biosynthesis of neoenterocins indicate a skeleton rearrangement of enterocin. *Org. Lett.* **2019**, *21*, 9066−9070.
(22) Zhang, Z.; Pan, H.-X.; Tang, G.-L. New insights into bacterial type II polyketide biosynthesis. *F1000Research* **2017**, *6*, No. 172.
(23) Kawasaki, T.; Hirashima, R.; Maruta, T.; Sato, H.; Maeda, A.; Yamada, Y.; Takeda, M.; Hayakawa, Y. Cloning and characterization of a gene cluster for hatomarubigin biosynthesis in *Streptomyces* sp. strain 2238-SVT4. *Appl. Environ. Microbiol.* **2010**, *76*, 4201−4206.
(24) Jumper, J.; Evans, R.; Pritzel, A.; Green, T.; Figurnov, M.; Ronneberger, O.; Tunyasuvunakool, K.; Bates, R.; Žídek, A.; Potapenko, A.; Bridgland, A.; Meyer, C.; Kohl, S. A. A.; Ballard, A. J.; Cowie, A.; Romera-Paredes, B.; Nikolov, S.; Jain, R.; Adler, J.; Back, T.; Petersen, S.; Reiman, D.; Clancy, E.; Zielinski, M.; Steinegger, M.; Pacholska, M.; Berghammer, T.; Bodenstein, S.; Silver, D.; Vinyals, O.; Senior, A. W.; Kavukcuoglu, K.; Kohli, P.; Hassabis, D. Highly accurate protein structure prediction with AlphaFold. *Nature* **2021**, *596*, 583−589.
(25) Pereira, P. J. B.; Macedo-Ribeiro, S.; Párraga, A.; Pérez-Luque, R.; Cunningham, O.; Darcy, K.; Mantle, T. J.; Coll, M. Structure of human biliverdin IX$\beta$ reductase, an early fetal bilirubin IX$\beta$ producing enzyme. *Nat. Struct. Biol.* **2001**, *8*, 215−220.
(26) Jiang, J.; Guiza Beltran, D.; Schacht, A.; Wright, S.; Zhang, L.; Du, L. Functional and structural analysis of phenazine *O*-methyltransferase LaPhzM from *Lysobacter antibioticus* OH13 and one-pot enzymatic synthesis of the antibiotic myxin. *ACS Chem. Biol.* **2018**, *13*, 1003−1012.
(27) Huber, T. D.; Wang, F.; Singh, S.; Johnson, B. R.; Zhang, J.; Sunkara, M.; Van Lanen, S. G.; Morris, A. J.; Phillips, G. N.; Thorson, J. S. Functional adomet isosteres resistant to classical adomet degradation pathways. *ACS Chem. Biol.* **2016**, *11*, 2484−2491.
(28) Chang, A.; Singh, S.; Bingman, C. A.; Thorson, J. S.; Phillips, G. N. Structural characterization of CalO1: a putative orsellinic acid methyltransferase in the calicheamicin-biosynthetic pathway. *Acta Crystallogr., Sect. D: Biol. Crystallogr.* **2011**, *67*, 197−203.
(29) Hertweck, C.; Luzhetskyy, A.; Rebets, Y.; Bechthold, A. Type II polyketide synthases: gaining a deeper insight into enzymatic teamwork. *Nat. Prod. Rep.* **2007**, *24*, 162−190.
(30) Zhou, H.; Li, Y.; Tang, Y. Cyclization of aromatic polyketides from bacteria and fungi. *Nat. Prod. Rep.* **2010**, *27*, 839−868.
(31) Shen, Y.; Yoon, P.; Yu, T.; Floss, H. G.; Hopwood, D.; Moore, B. S. Ectopic expression of the minimal *whiE* polyketide synthase generates a library of aromatic polyketides of diverse sizes and shapes. *Proc. Natl. Acad. Sci. U.S.A.* **1999**, *96*, 3622−3627.
(32) Lee, M.-Y.; Ames, B. D.; Tsai, S. Insight into the molecular basis of aromatic polyketide cyclization: Crystal structure and *in vitro* characterization of WhiE-ORFVI. *Biochemistry* **2012**, *51*, 3079−3091.
(33) Meurer, G.; Gerlitz, M.; Wendt-Pienkowski, E.; Vining, L. C.; Rohr, J.; Hutchinson, C. R. Iterative type II polyketide synthases, cyclases and ketoreductases exhibit context-dependent behavior in the biosynthesis of linear and angular decapolyketides. *Chem. Biol.* **1997**, *4*, 433−443.
(34) Matsuda, Y.; Gotfredsen, C. H.; Larsen, T. O. Genetic characterization of neosartorin biosynthesis provides insight into heterodimeric natural product generation. *Org. Lett.* **2018**, *20*, 7197−7200.
(35) Huang, C.; Yang, C.; Zhu, Y.; Zhang, W.; Yuan, C.; Zhang, C. Marine bacterial aromatic polyketides from host-dependent heterologous expression and fungal mode of cyclization. *Front. Chem.* **2018**, *6*, No. 528.
(36) Masters, K.-S.; Bräse, S. Xanthones from fungi, lichens, and bacteria: The natural products and their synthesis. *Chem. Rev.* **2012**, *112*, 3717−3776.


https://doi.org/10.1021/jacsau.2c00594
*JACS Au* 2023, 3, 195−203